J Therm Anal Calorim (2011) 103:853–862
DOI 10.1007/s10973-010-1065-5

Study on thermal decomposition of calix[6]arene and calix[8]arene

K. Chennakesavulu · M. Raviathul Basariya · G. Bhaskar Raju · S. Prabhakar

Received: 9 August 2010 / Accepted: 16 September 2010 / Published online: 9 October 2010
© Akadémiai Kiadó, Budapest, Hungary 2010

Abstract Thermal decomposition kinetics of calix[6]arene (C6) and calix[8]arene (C8) were studied by Thermogravimetry analysis (TG) and Differential thermal analysis (DTA). TG was done under static air atmosphere with dynamic heating rates of 1.0, 2.5, 5.0, and 10.0 K min^{-1}. Model-free methods such as Friedman and Ozawa–Flynn–Wall were used to evaluate the kinetic parameters such as activation energy (E_a) and pre-exponential factors (ln A). Model-fitting method such as linear regression was used for the evaluation of optimum kinetic triplets. The kinetic parameters obtained are comparable with both the model-free and model-fitting methods. Within the tested models, the thermal decomposition of C6 and C8 are best described by a three dimensional Jander's type diffusion. The anti-oxidant efficiency of C6 and C8 was tested for the decomposition of polypropylene (PP).

Keywords Calix[*n*]arenes · Thermal decomposition · Activation energy · Model-free and model-fitting methods · Jander's type diffusion

Introduction

Calix[*n*]arenes are macrocyclic baskets derived from condensation of phenol and formaldehyde in alkali media. Calix[*n*]arenes are extensively used in selective extraction of metals, nuclear waste treatment, catalysis, complexation of fullerenes and neutral molecules. Synthesis of calix[*n*]arenes and characterizing them by their physical properties such as melting point, solubility and acid dissociation constant (pK_a) is a challenging task [1, 2]. The higher melting points of calix[*n*]arenes necessitate a careful study of their thermal behaviour. Thermo kinetic analysis has been extensively applied in the field of polymers, solid/liquid interface, carbohydrate chemistry, minerals, energetic materials, pharmaceutical and biochemistry [3–5]. The TG analysis is a useful tool for the determination of inclusion behaviour of calix[n]arenes with guest molecules such as toluene, xylene, chloroform, acetone and alkyl ammonium [6, 7]. Calix[*n*]arenes are good antioxidants for the oxidation of polyolefins such as polypropylene, low-density polyethylene and high-density polyethylene [8–12]. It is reported that in USA alone, nearly twenty thousand tonnes of phenolic antioxidants were consumed during 1983 for the stabilization of plastics, it clearly reveals the importance of antioxidants in polymer industry [13]. The present study includes the results of the work carried out on the synthesis of calix[*n*]arenes and their thermal decomposition kinetics.

Experimental

Materials

The p-*tert*-butyl phenol, formaldehyde and para-formaldehyde used in the study are of analytical grade chemicals, whilst chloroform, toluene and xylene are of Merk Speciality grade.

K. Chennakesavulu (✉) · M. Raviathul Basariya · G. Bhaskar Raju · S. Prabhakar
National Metallurgical Laboratory Madras Centre, CSIR Madras Complex, Taramani, Chennai 600113, India
e-mail: chennanml@yahoo.com; chenna_velpumadugu@yahoo.com

Synthesis of calixarenes

5,11,17,23,29,35-Hexa-*tert*-butyl-37,38,39,40,41,42-hexa hydroxy calix[6]arene and 5,11,17,23,29,35,41,47-Octa-*tert*-butyl-49,50,51,52,53,54,55,56-octa hydroxy calix[8]-arene were synthesized as per the established procedure [14]. The calixarenes obtained were further de-*tert*-butylated using $AlCl_3$/Toluene media [15].

37,38,39,40,41,42-Hexa hydroxy calix[6]arene (C6): Melting point: 688–690 K, LCMS-ESI $(M-1)^+$: 635. Molecular Formulae: $C_{42}H_{36}O_6$, Calculated: (C, 79.22%) (H, 5.70%), Found: (C, 79.12%), (H, 5.29%). ^{1}H NMR (500 MHz, $CDCl_3$) δ (ppm): 10.3 (s, 6H, –OH), 7.1, 6.8 (m, 18H, Ar–H), 3.8 (s, 12H, Ar–CH_2–). ^{13}C NMR (500 MHz, pyridine-d5) δ (ppm): 152.9, 128.8, 123.2, 120.3, 32.7. DEPT-NMR (500 MHz, pyridine-d5) δ (ppm): 152, 128, 123.2, 120.3 (Aromatic –CH), 32.7 (Bridged methylene, –CH_2–). ^{13}C NMR CP-MAS (300 MHz) δ (ppm): 150, 128, 125, 120, 29.5.

49,50,51,52,53,54,55,56-Octa hydroxy calix[8]arene (C8): Melting point: 646–648 K, LCMS-ESI $(M-1)^+$: 847. Molecular Formulae: $C_{42}H_{36}O_6$, Calculated: (C, 79.22%), (H, 5.70%), Found: (C, 79.21%), (H, 5.98%). ^{1}H NMR (500 MHz, DMSO-d6) δ (ppm): 8.8 (s, 8H, –OH), 6.9, 6.6 (m, 24H, Ar–H), 3.8 (s, 16H, Ar–CH_2–). ^{13}C NMR (500 MHz, pyridine-d5) δ (ppm): 152.9, 128.8, 123.5, 120.4, 32.3. DEPT-NMR (500 MHz, pyridine-d5) δ (ppm): 149.9, 128.8, 123.5, 120.4 (Aromatic –CH), 32.3 (Bridged methylene, –CH_2–). ^{13}C NMR CP-MAS (300 MHz) δ (ppm): 148.6, 128.5, 120.4, 29.8.

Characterization

Bruker Avance-500 MHz NMR spectrometer was used to record the ^{1}H NMR, ^{13}C NMR, DEPT-NMR of the sample. Bruker Avance 300 MHz NMR spectrometer was used to record the ^{13}C NMR Cross Polarization Magic Angle Spinning Spectrum (CP-MAS). The samples were taken in 2.5 mm diameter zircon rotors and spun at 7 kHz. The elemental analysis of the sample was performed using Euro Vectors Elemental analyzer. FTIR spectra were recorded with Perkin Elmer FTIR instrument. HPLC and LCMS–ESI analyses were carried out using Schimadzu and Agilent technology instruments respectively. EPR spectra were recorded on a Bruker X-Band EMX-EPR instrument at room temperature with the modulation frequency set at 100 kHz and microwave power at 3.2 mW. The g value were measured against DPPH, $g = 2.0045 \pm 0.0002$, which was used as the external reference. The error in the reported g value is ± 0.0002.

Sample preparation

In order to study the thermograms of pure samples, prior to the TG experiments, the C6 and C8 were degassed at 500 K under vacuum (10^{-5} Torr) for 48 h. The removal of traces of solvent in calix[n]arenes, results in controlled TG signal as evidenced by a constant mass before the start of the melting of the sample.

Thermal analysis

TG/DTG experiments were performed with Versa Therm Cahn thermo balance TG-151 attached to an analytical thermal system. Thermal experiments were conducted in the temperature range of 300–1,100 K with samples weighing around 20 mg. The analyses were carried out at four nominal heating rates (1.0, 2.5, 5.0 and 10.0 K min^{-1}) under static air atmosphere. DTA was carried out using Netzsch 409C model instrument in static air atmosphere with heating rate of 10.0 K min^{-1} and with 20 mg of sample. The Netzsch Thermo kinetics software was used for kinetic analysis of experimental data.

Theoretical approach

The kinetics of solid single step thermal decomposition [16] is governed by the Eq. 1.

$$\frac{d\alpha}{dt} = k(T)f(\alpha) \tag{1}$$

where α is the conversion of the reaction, $d\alpha/dt$ rate of conversion, $f(\alpha)$ reaction model and $k(T)$ is the temperature-dependent rate constant, respectively.

The fractional conversion α which is applicable to TG data is expressed $(m_0 - m_t)/m_0 - m_f)$, where m_0, m_f are the initial and final mass of the sample and m_t is the mass of the sample at time t. The explicit temperature dependence of the rate constant is described according to the Arrhenius Eq. 2.

$$k(T) = A\exp\left(-\frac{E_a}{RT}\right) \tag{2}$$

By combining the Eqs. 1 and 2 the following is obtained.

$$\frac{d\alpha}{dt} = A\exp\left(\frac{-E_a}{RT}\right)f(\alpha) \tag{3}$$

where A is the pre-exponential factor (rate constant at infinite temperature), R is the gas constant, E_a is the apparent activation energy and T is the absolute temperature. According to non-isothermal kinetic theory, the fractional conversion (α) can be expressed as a function of temperature, which is dependent on the time of heating.

The explicit time dependence of Eq. 3 can be eliminated through the trivial transformation and is expressed by Eq. 4, which is valid only for constant heating rate.

$$\frac{d\alpha}{dt} = \frac{1}{\beta} A \exp\left(\frac{-E_a}{RT}\right) f(\alpha) \quad (4)$$

where $\beta = dT/dt$ is the heating rate.

Kinetic parameter calculations based on TG data can be obtained from Eqs. 3 and 4. In the present study, two different approaches namely Model-free methods [17–19] and Model-based methods [20–22] were used to calculate the kinetic parameters. The kinetic parameters obtained using non-isothermal TG was observed to be advantageous over conventional isothermal studies [23].

Model-free or isoconversional method

In order to gain more information regarding the decomposition mechanism, model-free methods which are recommended as a trustworthy were adopted for kinetic analysis. The basic assumption of the model-free method is that the kinetic triplet is independent on the heating rate. The activation energy values calculated by this method are independent of any implicit reaction model, which allows one to explore multi-step kinetics [24]. The most common model-free methods such as Friedman and Ozawa–Flynn–Wall were employed for the thermo-kinetic analysis of calix[*n*]arenes.

Friedman method

The method [17] based on the inter comparison of the rate of conversion $d\alpha/dt$ for a given degree of conversion α

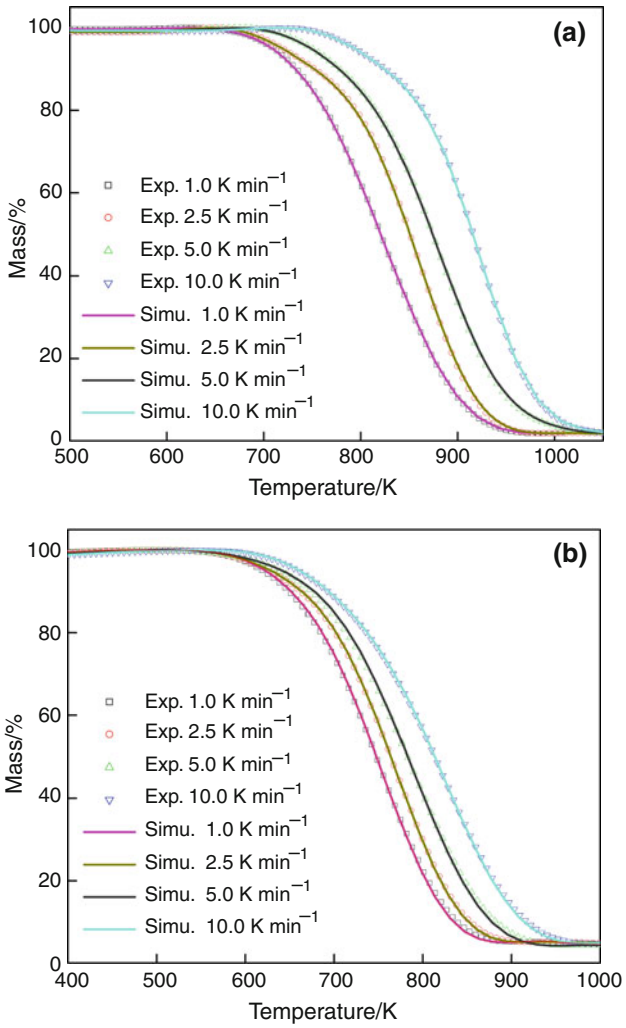

Fig. 1 Experimental and simulated non-isothermal TG curves of **a** C6, **b** C8

Table 1 Algebraic expression for $f(\alpha)$ and $g(\alpha)$ for the various kinetic reaction models

S. no.	Reaction model	Code	$f(\alpha)$	$g(\alpha)$
1	First order	F1	$(1-\alpha)$	$-\ln(1-\alpha)$
2	Second order	F2	$(1-\alpha)^2$	$(1-\alpha)^{-1}-1$
3	Third order	F3	$(1-\alpha)^3$	$0.5(1-\alpha)^{-2}-1$
4	Avrami Erofeev eq.	A2	$2(1-\alpha)[-\ln(1-\alpha)]^{1/2}$	$[-\ln(1-\alpha)]^{1/2}$
5	Avrami Erofeev eq.	A3	$3(1-\alpha)[-\ln(1-\alpha)]^{2/3}$	$[-\ln(1-\alpha)]^{1/3}$
6	Avrami Erofeev eq.	An	$n(1-\alpha)[-\ln(1-\alpha)]^{(1-1/n)}$	$[-\ln(1-\alpha)]^{1/n}$
7	Prout-Tomkins eq	B1	$\alpha(1-\alpha)$	$\ln[\alpha/(1-\alpha)]$
8	1D diffusion	D1	$1/2\alpha$	$(\alpha)^2$
9	2D diffusion	D2	$[-\ln(1-\alpha)]^{-1}$	$\alpha+[(1-\alpha)\ln(1-\alpha)]$
10	Jander's equation	D3	$(3/2)(1-\alpha)^{2/3}[1-(1-\alpha)^{1/3}]^{-1}$	$[1-(1-\alpha)^{1/3}]^2$
11	Ginstling-Brounshtein	D4	$(3/2)[(1-\alpha)^{-1/3}-1]^{-1}$	$[1-2\alpha/3]-(1-\alpha)^{2/3}$
12	2D phase boundary	R2	$2(1-\alpha)^{1/2}$	$[1-(1-\alpha)^{1/2}]$
13	3D phase boundary	R3	$3(1-\alpha)^{2/3}$	$[1-(1-\alpha)^{1/3}]$

determined using dynamic heating rate β is considered as the most general derivative technique.

After taking logarithms of Eq. 4 and rearranging, we obtain

$$\ln\left(\beta\frac{\mathrm{d}\alpha}{\mathrm{d}T}\right) = \ln[Af(\alpha)] - \frac{E_a}{RT} \quad (5)$$

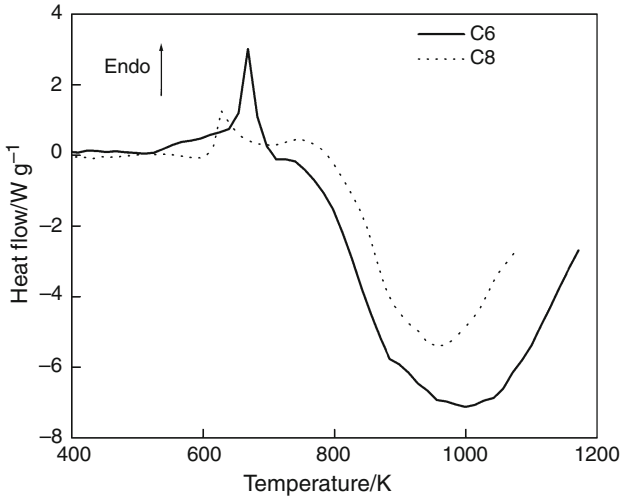

Fig. 2 DTA curves of C6 and C8 (heating rate: 5 K min^{-1})

The activation energy (E_a) values over a wide range of conversions was obtained by plotting $\ln\left(\beta\frac{\mathrm{d}\alpha}{\mathrm{d}T}\right)$ versus $1/T$ for a constant α value.

Ozawa–Flynn–Wall method

This method [18, 19] is an integral method which can determine the activation energy without the knowledge of reaction order for given values of conversion.

Integrating Eq. 4 and rearranging, we obtain

$$\log\beta = \log\frac{AE_a}{g(\alpha)R} - 2.314 - \frac{0.4567E_a}{RT} \quad (6)$$

where

$$g(\alpha) = \int_0^{\alpha}\frac{\mathrm{d}\alpha}{f(\alpha)} \quad (7)$$

By plotting log β against $1/T$ at certain conversion rate, the slope $-E_a/R$ indicate the activation energy.

Model-fitting method

The model-based kinetic analysis depends on the reaction type and reaction model. The reaction model may take

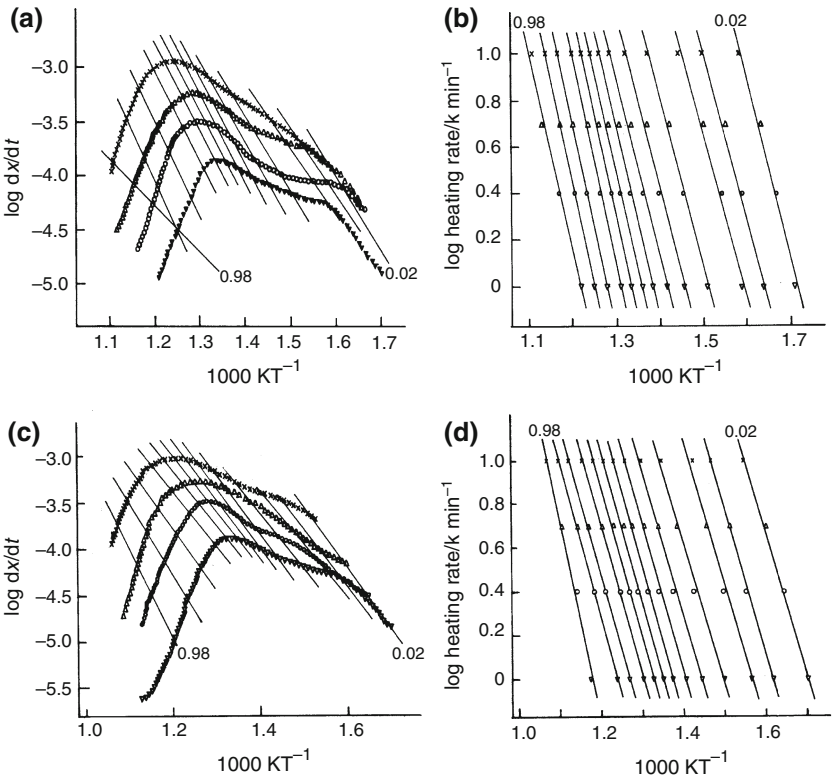

Fig. 3 Model-free plots of **a** Friedman analysis of C6, **b** Ozawa–Flynn–Wall analysis of C6, **c** Friedman analysis of C8, **d** Ozawa–Flynn–Wall analysis of C8

various forms based on nucleation and nucleus growth, phase boundary reaction, diffusion and chemical reaction. The model with selected reaction types gives quite reliable and consistent kinetic parameters. The unknown parameters were found from the fitting of measured data with the simulated curves for the given model and reaction types. The different kinetic reaction models [25] used for the analysis to identify the best reaction model is represented in Table 1.

Results and discussion

TG/DTA analysis

The experimental TG curves corresponding to the thermal mass loss of C6 and C8 are shown in Fig. 1. The thermal decomposition of C6 occurred between 660 and 900 K with a mass loss of 95%. In the case of C8, the decomposition occurred between 630 and 900 K with a mass loss

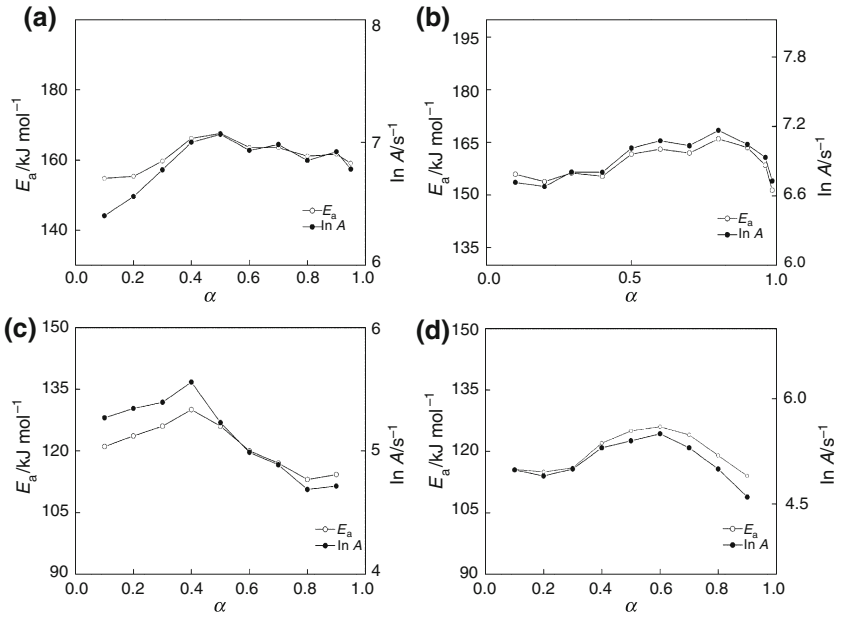

Fig. 4 **a** Energy plot of Friedman for C6, **b** energy plot of Ozawa–Flynn–Wall for C6, **c** energy plot of Friedman for C8, **d** energy plot of Ozawa–Flynn–Wall for C8. The values are evaluated using F1 kinetic model

Table 2 Kinetic triplets of C6 and C8 for the tested models with linear regression

Code	Calix[6]arene					Calix[8]arene				
	E_a/kJ mol^{-1}	ln A/s^{-1}	r^2	σ		E_a/kJ mol^{-1}	ln A/s^{-1}	r^2	σ	
				E_a	ln A				E_a	ln A
F1	111	4.6	0.9954	5.1	0.27	99	3.7	0.9980	2.8	0.14
F2	136	6.7	0.9964	6.2	0.32	124	5.7	0.9982	3.1	0.16
F3	126	5.9	0.9969	6.0	0.31	110	4.5	0.9987	2.7	0.14
A2	98	3.7	0.9802	6.1	0.32	85	2.7	0.9869	4.4	0.23
A3	99	3.9	0.9704	4.8	0.25	86	2.7	0.9787	4.2	0.22
An	152	7.5	0.9979	4.4	0.23	121	5.2	0.9980	2.1	0.11
B1	113	5.9	0.9529	7.6	0.43	98	4.7	0.9634	2.7	0.14
D1	132	5.6	0.9985	0.9	0.08	118	4.5	0.9987	1.2	0.10
D2	141	6.1	0.9990	1.2	0.06	127	5.0	0.9991	1.5	0.08
D3	165	6.6	0.9998	0.5	0.02	127	5.5	0.9999	0.7	0.06
D4	145	5.8	0.9992	2.1	0.11	132	4.7	0.9992	2.2	0.11
R2	105	3.8	0.9918	4.2	0.22	92	2.8	0.9957	3.1	0.16
R3	107	3.8	0.9930	5.0	0.26	94	2.8	0.9967	3.2	0.16

of 95%. It is interesting to note that both C6 and C8 follows a single stage decomposition. The three step decomposition mechanism was observed for thermal decomposition of calix[4]arene, azacalix[4]arene and p-*tert*-butyl calix[4] arenes. The first step corresponds to the loss of entrapped methanol molecules and melting of compounds with simultaneous two step decomposition process [26]. The DTA of C6 and C8 are shown in Fig. 2. In the case of C6, an endothermic peak was observed around 670 K indicating the melting of the C6. The exothermal peak above 700 K indicates the cleavage of methylene group from phenolic arene groups. Similarly, an endothermic peak observed around 630 K indicates the melting of sample and the exothermal peak above this temperature shows cleavage of C8 cavity. The strong influence of the atmospheric condition on exothermal decomposition of calix[4]arene was reported [26].

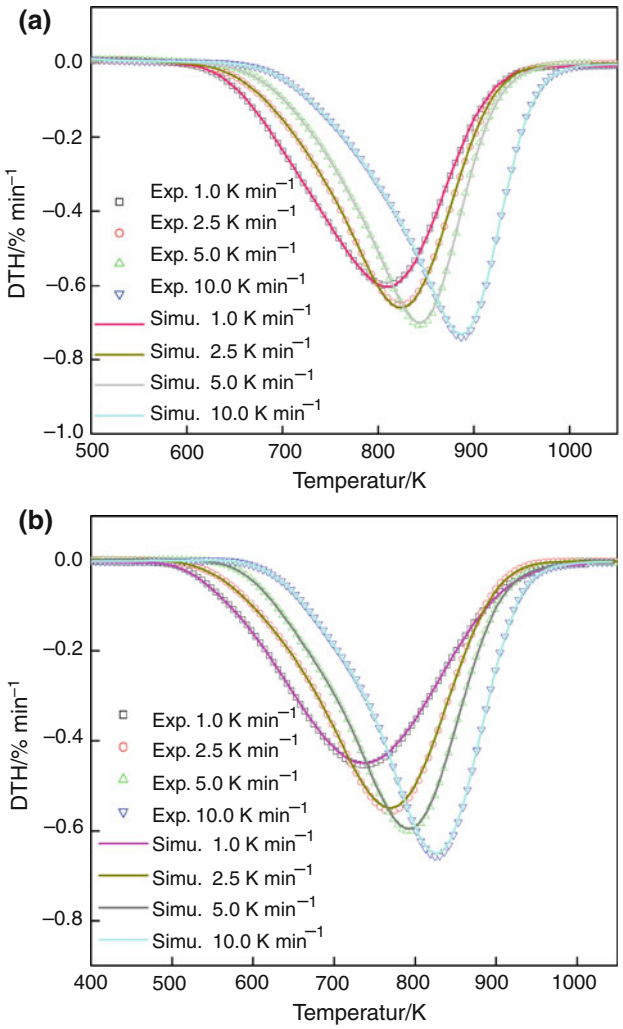

Fig. 5 Fit of experimental and simulated DTG curves obtained for the reaction type D3 **a** C6, **b** C8

Model-free analysis

The Friedman and Ozawa–Flynn–Wall analysis for the thermal decomposition reaction of C6 and C8 and their corresponding energy plots were shown in Figs. 3 and 4 respectively. These plots shows good linearity with little scattering at the beginning and end of the plots. The differential Friedman method indicates an average E_a value of 161 kJ mol^{-1} for C6 with standard deviation (σ) of 4.1 and 121 kJ mol^{-1} ($\sigma = 5.7$) for C8. Similar results with an average E_a value of 159 kJ mol^{-1} ($\sigma = 4.6$) for C6 and 119 kJ mol^{-1} ($\sigma = 4.7$) for C8 were observed while using Ozawa–Flynn–Wall method. From the results shown in Fig. 3, it is clear that Ozawa–Flynn–Wall straight lines fitted at different conversion rates are almost parallel indicating the best fit of this method to our system [27]. Figure 4 shows the plots of activation energy and pre-exponential factor as a function of fractional conversion where $\alpha = 0.1$–0.9 for C6 and C8. It reveals the linear dependence of activation energy with the pre-exponential factor. As the thermal decomposition proceeds, the activation energy remains almost same with an error limit of ± 5 kJ mol^{-1}.

Model-fitting analysis

Linear regression models were used for the evaluation of kinetic parameters. Most probable kinetic model is analyzed by choosing best fit based on the value of the

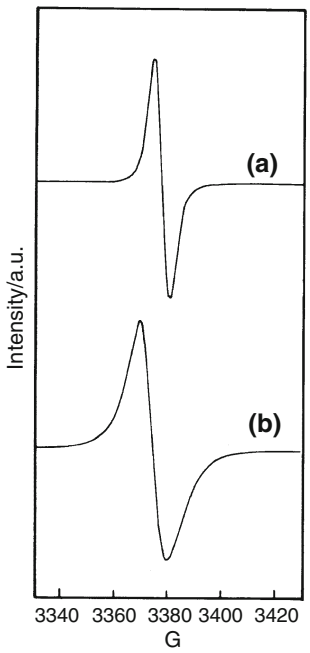

Fig. 6 EPR spectrum of TGA quenched **a** C6 at 745 K, **b** C8 at 715 K

correlation coefficient r^2 which is close to one. The activation energies and correlations corresponding to different mechanism for linear regression method for C6 and C8 are shown in Table 2. Among the tested models, the C6 and C8 obeyed the diffusion mechanism namely D3, (model 10) the Jander's type with integral form $g(\alpha) = [1 - (1 - \alpha)^{1/3}]^2$ and differential form $(3/2)(1 - \alpha)^{2/3}[1 - (1 - \alpha)^{1/3}]^{-1}$. Figure 5 shows the fitted curve for linear regression of the DTG kinetic data for a single step degradation of C6 and C8, which invokes 3D diffusion. In order to check the validation of kinetic parameters the experimental TG curves are compared with simulated TG curves obtained using D3 reaction model as shown in Fig. 1. Using the activation energy data, we found the values obtained using model-free and model-based methods were close to each other. Therefore, the determined activation energies are reasonable and can be applied to arrive at the best kinetic models for C6 and C8.

EPR analysis

The ESR spectra of TG quenched solid C6 and C8 were shown in Fig. 6. The symmetrical singlets of ESR spectra could be explained due to the formation of isotropic free radicals. The g factor was measured to be 2.00324 for C6 and 2.0362 for C8. The effect of pyrolysis temperature on EPR signal of primary radicals formed during the pyrolysis of tobacco was reported [28]. The results confirm that at lower temperature the most resolved spectra were obtained, where at higher temperatures the broadened spectra were obtained. The free radicals of water soluble calix[n]arenes do not exhibit their hyperfine interaction, because the radical centre is in the –OH groups of calix[n]arenes cavity [29]. Generation of free radical was observed when 5,11,17,23-tetrabromo-25,26,27,28-tetramethoxy calix[4]-arene was subjected to UV irradiation [30]. In the present study, the quenched samples were kept for 1 week and

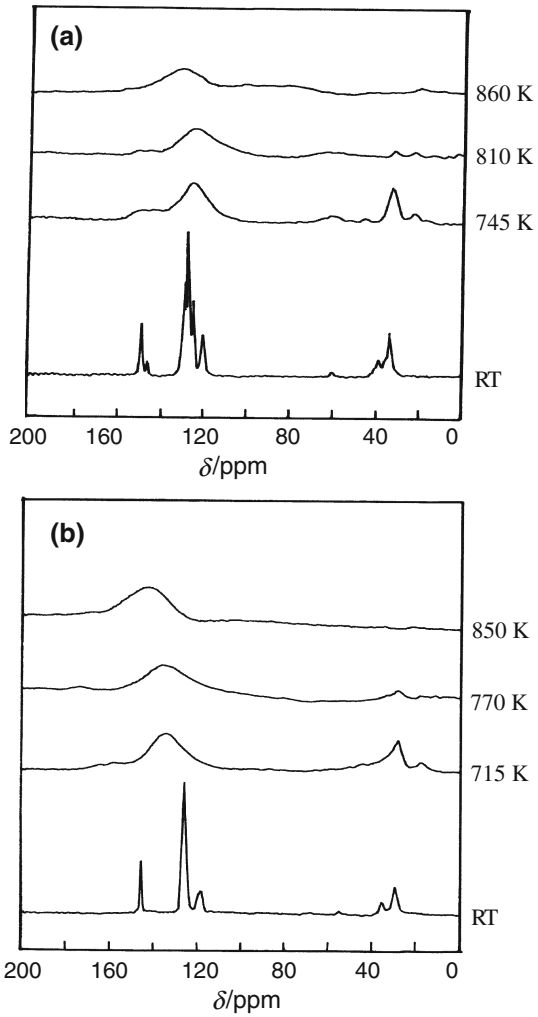

Fig. 7 ^{13}CNMR CP-MASS of TGA quenched **a** C6 and **b** C8 at various temperatures

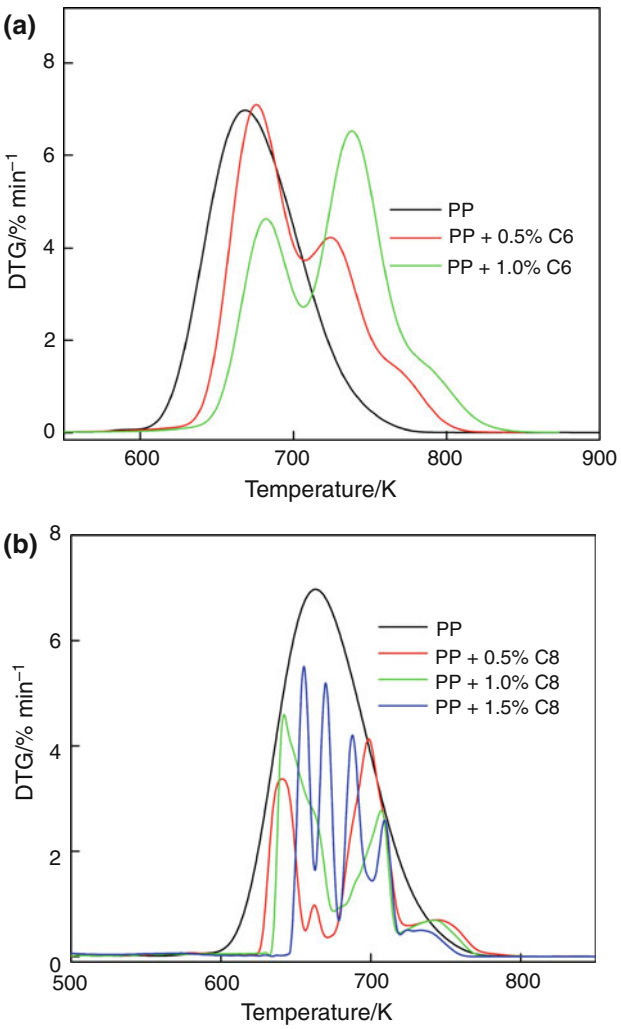

Fig. 8 DTG of polypropylene with C6 and C8 as a antioxidant additive (heating rate: 5 K min^{-1})

their EPR spectra were taken. The EPR signals were noticed even after 1 week. Thus it is apparent that the free radicals generated are very stable.

^{13}CNMR CP-MAS analysis

The ^{13}CNMR CPMAS of C6 and C8 at room temperature and quenched at various temperatures were shown in Fig. 7. It is apparent that at room temperature, the aromatic carbon signals were observed from 150 to 120 ppm where as signals corresponding to bridged methylene carbons were observed at 29.5 ppm. In the case of quenched C6 and C8 at various temperatures, the signals corresponding to aromatic carbons were broadened drastically. This could be attributed to the formation of stable phenoxy free radical. The delocalization of free electron throughout the arene ring may lead to the broadening of signal in ^{13}CNMR CP MAS. Qin et al. reported that the formation of free radicals within apocynum fiber, results in broader peaks in ^{13}CNMR CP MAS [31]. The bridged methylene signals were shifted and almost disappeared at higher temperatures. This indicates the cleavage of methylene bridge from its phenolic groups.

Antioxidant efficiency of C6 and C8

TG of polypropylene was done in the absence and presence of C6 and C8, the results were presented in the form of DTG in Fig. 8. The DTG curve of polypropylene (PP) suggests the decomposition of PP occurs in single step in the range of 600–800 K. In the presence of C6 the single step DTG curve of PP shows two step decomposition. It is evident that during decomposition of PP the C6 is exhibiting its antioxidant activity. Similarly, in the presence of C8 the single step DTG curve of PP becomes multi-step decomposition. The FTIR coupled with mass spectroscopy study revealed the formation of less stable primary and secondary radicals, when PP was subjected to decomposition [32]. These radicals may gain hydrogen atom from phenolic groups of C6 or C8 and form paraffins. Thus the presence of C6 and C8 prevents the decomposition of PP. Generally, the efficiency of antioxidant capacity depends on the ring size due to the effect induced by the phenolic groups, the spatial protections of double bond by delocalization of π-electrons and the interaction of oxygen atoms of OH units and the trapped radicals [10]. The decomposition mechanism of PP in the presence of calix[*n*]arene

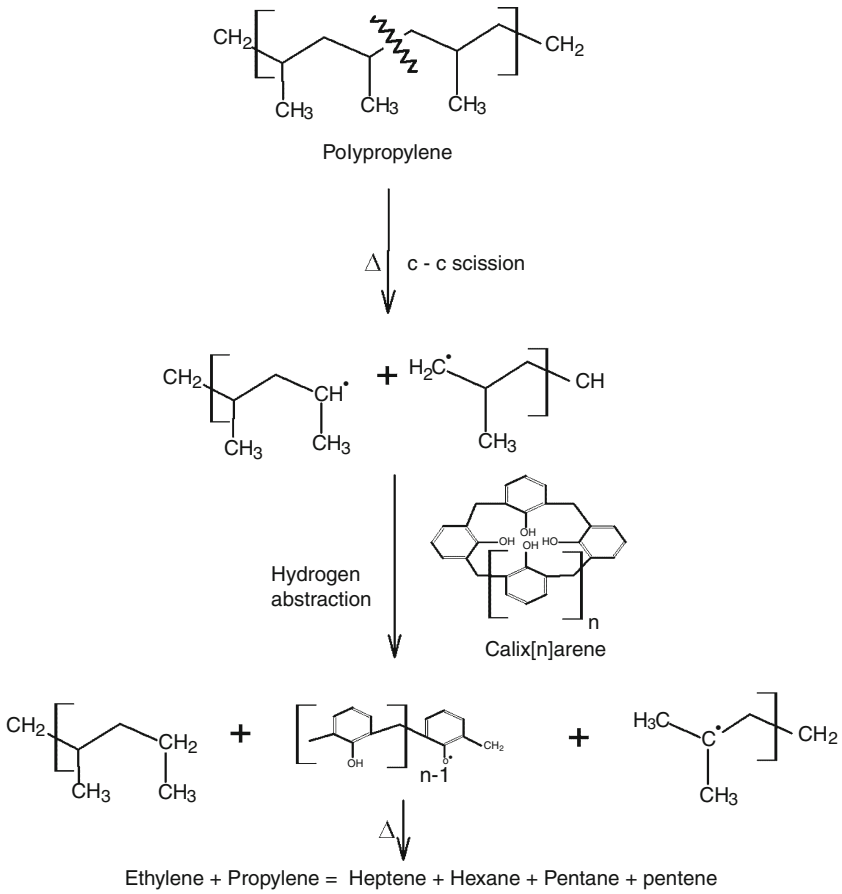

Fig. 9 Decomposition prevention mechanism of PP in presence of calix[*n*]arene

was shown in Fig. 9. The E_a values of water soluble calix[*n*]arenes revealed lowering of E_a value with increasing the ring size [33]. The E_a value varies with the addition of PP during the pyrolysis of oil shale indicates the accelerated decomposition of oil shale [34]. The E_a values help us to estimate the efficiency of antioxidant capacity. Based on the ring size and its lower E_a, C8 was observed to be better antioxidant compared to C6.

Conclusions

Thermal decomposition of C6 and C8 follows the single stage with a Jander's type diffusion mechanism. The kinetic study showed that the E_a values of C6 obtained by Friedman and Ozawa–Flynn–Wall methods were 161 and 159 kJ mol^{-1} respectively, with ln *A* of 6.8 s^{-1} and in the case of C8 the E_a values are 121 and 119 kJ mol^{-1} respectively, with ln *A* of 5.1 s^{-1}. The EPR and ^{13}CNMR CP-MAS confirm the formation of open chain poly phenolic free radicals during decomposition of C6 and C8. The higher antioxidant efficiency of C8 with PP was observed when compared to C6. In presence of calix[*n*]arene the decomposition mechanism of polypropylene was proposed.

Acknowledgements The authors K. Chennakesavulu and M. Raviathul Basariya Senior Research Fellows are grateful to Council of Scientific and Industrial Research (CSIR), New Delhi (India) for financial support. The authors are grateful to SAIF-NMR Facility, Indian Institute of Technology, Madras (India), NMR Centre-Indian Institute of Science, Bangalore (India) for providing the necessary spectral and analytical data.

References

1. Gutsche CD. Calixarenes. Monographs in supramolecular chemistry. London: Royal Society of Chemistry; 1989.
2. Asfari Z, Bohmer V, Harrowfield J, Vicens J, Saadioui M. Calixarenes 2001. Netherlands: Kluwer Academic Publishers; 2001.
3. Radhakrishnan Nair MN, Thomas GV, Gopinathan Nair MR. Thermogravimetric analysis of PVC/ELNR blends. Polym Degrad Stab. 2007;92:189–96.
4. Yao F, Wu Q, Lei Y, Guo W, Xu Y. Thermal decomposition kinetics of fibers: activation energy with dynamic thermo gravimetric analysis. Polym Degrad Stab. 2008;93:90–8.
5. Vyazovkin S. Thermal analysis. Anal Chem. 2008;80:4301–16.
6. Lazzarotto M, Nachtigall FF, Schnitzler E, Castellano EE. Thermo gravimetric analysis of supramolecular complexes of p-tert-butylcalix[6]arene and ammonium cations: crystal structure of diethylammonium complex. Thermochim Acta. 2005;429:111–7.
7. Schatz J, Schildbach F, Lentz A, Rastatter S. Thermal gravimetry, mass spectrometry and solid-state ^{13}C NMR spectroscopy-simple and efficient methods to characterize the inclusion behavior of p-tert-butylcalix[n]arenes. J Chem Soc Perkin Trans 2. 1998;(1):75–7.
8. Pastor SD, Odorisio P. Acylated calixarene stabilizers. US Patent 4,617,336. 1986.
9. Seiffarth K, Schulz M, Gormar G, Bachmann J. Calix[n]arenes-new light stabilizers for polyolefins. Polym Degrad Stab. 1989;24:73–80.
10. Feng W, Yuan LH, Zheng SY, Huang GL, Qiao JL, Zhou Y. The effect of p-tert-butylcalix[n]arene on γ-radiation degradation of polypropylene. Radiat Phys Chem. 2000;57:425–9.
11. Zaharescu T, Jipa S, Setnescu R, Santos C, Gigante B, Mihalcea I, Podina C, Gorghiu LM. Thermal stability of additivated isotactic polypropylene. Polym Bull. 2002;49:289–96.
12. Jipa S, Zaharescu T, Setnescu R, Setnescu T, Dumitru M, Gorghiu LM, Mihalcea I, Bumbac M. Effect of calixarenes on thermal stability of polyethylenes. Polym Degrad Stab. 2003;80:203–8.
13. Pospisil J. Mechanistic action of phenolic antioxidants in polymers—a review. Polym Degrad Stab. 1988;20:181–202.
14. Gutsche CD, Dhawan B, No KH, Muthukrishnan R. Calixarenes. 4. The synthesis, characterization and properties of the calixarenes from p-tert-butylphenol. J Am Chem Soc. 1981;103:3782–92.
15. Gutsche CD, Lin LG. Calixarenes 12: the synthesis of functionalized calixarenes. Tetrahedron. 1986;42(6):1633–40.
16. Galwey AK, Brown ME. Handbook of thermal analysis and calorimetry, vol. 1. Amsterdam: Elsevier; 1998.
17. Friedman H. Kinetics of thermal degradation of char-forming plastics from thermogravimetry. Application to a phenolic plastic. J Polym Sci. 1963;6(1):183–95.
18. Ozawa T. A new method of analyzing thermogravimetric data. Bull Chem Soc Jpn. 1965;38:1881–6.
19. Flynn JH, Wall LA. General treatment of the thermogravimetry of polymers. J Res Natl Bur Stand. 1996;70A:487–523.
20. Vyazovkin S, Wight CA. Model-free and model-fitting approaches to kinetic analysis of isothermal and non-isothermal data. Thermochim Acta. 1999;340–341:53–68.
21. Swain SN, Rao KK, Nayak PL. Biodegradable polymers part II. Thermal degradation of biodegradable plastics cross-linked from formaldehyde-soy protein concentrate. J Therm Anal Calorim. 2005;79:33–8.
22. Turmanova SC, Genieva SD, Dimitrova AS, Vlaev LT. Non-isothermal degradation kinetics of filled with rise husk ash polypropene composites. Exp Polym Lett. 2008;2(2):133–46.
23. Chen F, Sorensen OT, Meng G, Peng D. Thermal decomposition of $BaC_2O_4.5H_2O$ Studied by stepwise isothermal analysis and non-isothermal thermogravimetry. J Therm Anal Calorim. 1998;53:397–410.
24. Vyazovkin S. A unified approach to kinetic processing of non-isothermal data. Int J Chem Kinet. 1996;28:95–101.
25. Pielichowski K, Njuguna J. Thermal degradation of polymeric materials. UK: Rapra Technology Limited; 2005.
26. Deligoz H, Ozen O, Cilgi GK, Cetisli H. A study on the thermal behaviours of parent calix[4]arenes and some azocalix[4]arene derivatives. Thermochim Acta. 2005;426:33–8.
27. Zhu L, Chen J, Xu L, Lian X, Xu K, Chen M. Synthesis of 3,5-ditert-butyl-4-hydroxybenzoates and their thermal antioxidation behavior for polypropylene. Polym Degrad Stab. 2009;94:1906–13.
28. Maskos Z, Khachatryan L, Dellinger B. Formation of the persistent primary radicals from the pyrolysis of tobacco. Energy Fuels. 2008;22:1027–33.
29. Tanaka A, Yashiro H, Ishigaki A, Murai H. Time-resolved ESR study on complex radical pairs formed in the photolysis of methylene blue included in water-soluble sulfonated calixarenes. Appl Magn Reson. 2010;37:581–93.
30. Wang Q, Li Y, Wu GS. ESR study of calix[4]arene by spin-trapping method. Appl Magn Reson. 2000;18:419–24.
31. Qin Z, Xin Z, Jian-Bing Z, Jun T, Zhao-Tian F, Wan-Fu S. Radiation effect of Apocynum fiber. Nucl Sci Tech. 2006;17:38–42.

32. Hedrick SA, Chuang SSC. Temperature programmed decomposition of polypropylene: in situ FTIR coupled with mass spectroscopy study. Thermochim Acta. 1998;315:159–68.
33. Yang W, Manek R, Kolling WM, Brits M, Liebenberg W, De Villiers MM. Physicochemical characterization of hydrated 4-sulphonato-calix[n]arenas: thermal, structural and sorption properties. Supramol Chem. 2005;17:485–96.
34. Aboulkas A, Harfi KE, Bouadili AE, Chanaa MB, Mokhlisse A. Pyrolysis kinetics of polypropylene morocco oil shale and their mixture. J Thermal Anal Calorim. 2007;89:203–9.